SIMULTANEOUS MEASUREMENT OF TURBULENT MOMENTUM AND MASS FLUXES IN CHANNEL FLOW OF VISCOELASTIC FLUID

Shumpei Hara
Department of Energy and Mechanical Engineering
Doshisha University
1-3 Tatara Miyakodani, Kyotanabe-shi, Kyoto 610-0394
shhara@mail.doshisha.ac.jp

Takahiro Tsukahara
Department of Mechanical Engineering
Tokyo University of Science
2641 Yamazaki, Noda, Chiba 278-8510
tsuka@rs.tus.ac.jp

Yasuo Kawaguchi
Department of Mechanical Engineering
Tokyo University of Science
2641 Yamazaki, Noda, Chiba 278-8510
yasuo@rs.noda.tus.ac.jp

ABSTRACT

In this experimental study, mass transfer characteristics in a turbulent channel flow of viscoelastic fluid was investigated by simultaneous particle image velocimetry and planar laser-induced fluorescence measurements. Instantaneous dye concentration field with fluctuating velocity vector showed spatial phase modulation in the streamwise velocity fluctuation and the dye concentration for the wall-normal velocity fluctuation. In addition, it was observed that hierarchically large-scale wavy motions with inclination transfer mass. A spatial spectral analysis allowed us to understand a higher wall-normal turbulent mass flux of low wave-number modes in the log-layer takes important role in comparison with the Reynolds shear stress. The existence of this characteristic wavy motion explains why the thinner dye concentration layer enhanced the magnitude of dye concentration fluctuation.

INTRODUCTION

The experimental report of turbulent channel flow, a canonical flow, can be used to benchmark and fine tune numerical simulations in initial step, and so indirectly contributes to the advancement of practical applications. The experimental report needs to include not only turbulence statistics but also instantaneous velocity and/or scalar fields as one of temporal-spatial information. For this thing, there is important to obtain the qualitative nature of the turbulence structure such as the streaky structure and the quantitative characteristics of its frequency and/or wave number calculated by the spectra analysis. Great performance of the numerical simulation according to the guideline of these facts provided from the experiment leads to fulfill practical demand: a precise estimation of the wall shear stress or heat and mass transfer coefficients determined by the turbulent mixing and diffusion. Whereas a comprehensive experimental database in channel flow of Newtonian fluid is enriched by a lot of effort (e.g., Adrian *et al.* (2000); del Álamo & Jiménez (2003); Gnielinski (1976); Kays (2012)), this usage is unfortunately restricted for non-Newtonian fluid, especially viscoelastic fluid.

Virk (1975) proposed a three-layer model of the mean velocity profile of a viscoelastic fluid flow, but this model was still not enough to adopt all cases in the experiment. This matter arose from a lack of understanding of the modulated turbulence structure appearing in this flow, and so past studies (e.g., Ptasinski *et al.* (2003); White & Mungal (2008)) have been mainly concentrated on an acquisition of the velocity field and turbulence statistics to get a clue. As a result, its overall picture has been gradually described. The scalar transfer closely associated with this structure is also profoundly important to underlie the calculation of transfer coefficients. Li *et al.* (2004) have reported the mean temperature profile by the fine-wire thermocouple for a turbulent channel flow of the viscoelastic fluid. They revealed an intensive temperature fluctuation in the log-layer with a high temperature gradient as well. As the next step it is reasonable to consider a spatial information of the scalar field in experimental report. Somandepalli *et al.* (2010) and Fu *et al.* (2014) have reported the spatial distribution of mass transport by simultaneous particle image velocimetry (PIV) and planar laser-induced fluorescence (PLIF) measurements for a channel flow and for a turbulent boundary layer flow, respectively. In their studies, the injection of a viscoelastic solution including dye into the Newtonian fluid flow from one sidewall has made the complicated flow situation of coexistence of both fluids. On the one hand, it is required to provide the experimental report for the instantaneous scalar field in a turbulent channel flow of the viscoelastic fluid used in the initial step of the benchmark test. However, as far as we are aware of, there is no experimental report to deal with this.

The present work performs simultaneous PIV and PLIF measurements in a turbulent channel flow of viscoelastic fluid in order to acquire the spatial scalar field. The authors have already reported fundamental turbulent statistics on velocity and concentration fluctuations (Matsumoto *et al.* (2017)). Following the previous result, Reynolds shear stress and wall-normal turbulent mass flux in a spectral description, which can evaluate the spatial scale of the turbulent mixing and diffusion in momentum and mass transfer quantitatively, will be the main focus of the present contribution.

EXPERIMENTAL APPARATUS AND SET-UP

Figure 1 summarizes schematic diagram of simultaneous PIV and PLIF measurements in a closed-circuit water loop including a plane channel which is of a height of $2h = 40$ mm and spanwise width of 500 mm. The dimensions of the dosing wall are 478×1498 mm^2; the permeable wall attached to one sidewall of the channel is made of laminated stainless-steel mesh. PIV and PLIF measurements are performed simultaneously on the *x*-*y* plane 3642 mm downstream from the channel entrance, where the mean velocity profile is fully developed and the boundary layer of the dye concentration is developing along the channel. Here, the instantaneous velocity field in the streamwise direction, x, and the wall-normal direction, y is named as u and v. We perform the experiments of flows of water (Newtonian fluid) and 25-ppm CTAC surfactant solution prepared with the same weight concentration of NaSal (viscoelastic fluid). The dosed fluid includes Rhodamine-WT of 1 ppm for the PLIF measurement. The Schmidt number, Sc, of the Rhodamine-WT is estimated as 4.7×10^3 from previous reports (Gillis *et al.* (2000); Benson *et al.* (2010)). The solution temperatures are controlled at 298.2±0.2 K. The dosed ratio of the dyed solution is set to 3.0×10^{-4} to minimize the disturbance of the dosed flow. Turbulence statistic quantities are calculated from 1000 instantaneous images of 54×40 mm^2 space. The values of key parameters in our experiments are provided in Table 1. The Reynolds number, Re, is defined as $2hU_b/\nu$. Here, ν is the kinetic viscosity and U_b is the bulk mean velocity calculated from flow rate measured by an electromagnetic flow meter. In the inner units, the friction velocity is u_τ (= $\sqrt{\tau_w/\rho}$, where τ_w is the wall shear stress estimated from the pressure difference between pressure taps installed on the channel wall across the PIV and PLIF measurement area and ρ is the fluid density) and the friction concentration is c_τ calculated by extrapolation from wall-normal turbulent mass flux distribution. In the present study, it is noted that averaged and fluctuating components of dye concentration, c, are converted with the value at the wall. Hereafter, the superscripts $(\ \ )'$, $\overline{(\ \ )}$, and $(\ \ )^+$ denote fluctuating component, temporal-spatial-averaged value, and normalization with the inner units, respectively. Interest in this paper is in the near-wall region, so the inner units are basically used for normalization.

AVERAGED VELOCITY AND DYE CONCENTRATION PROFILES

Before discussing in the detail about fundamental turbulence statistics, averaged velocity and dye concentration profiles in semi-logarithmic plot are introduced in Figs. 2 and 3 to examine those gradients and the thickness of a dye concentration layer. In the figure 3, c_w is calculated from dosing rate, dosing area, and the wall mass flux which is extrapolated from the slope of five points beyond the peak value in wall-normal turbulent mass flux distribution as well as c_τ. c_∞ is the dye concentration at the 99%-thickness of the boundary layer. DNS results (Iwamoto *et al.* (2002) and Kozuka *et al.* (2009)) are presented in the figure to evaluate the accuracy for the measurement. Also the velocity profile for a laminar flow and Virk's ultimate profile Virk (1975) are given to compare drag reduction level.

The result of averaged streamwise velocity profile for Newtonian fluid flow is good agreement with the DNS result. As the experimental accuracy of the PIV system set up is satisfactory, so we can say that the inner region covering the viscous sub-layer, buffer layer, and logarithmic layer is visible in the result. The measured dye concentration distribution for $y^+ \leq 70$ deviates from the DNS result due to various condition differences in the present experiment such as the boundary condition of the scalar field, Sc and Pr, and Re. However the outer part of the turbulent region shows better agreement with the DNS data. In this region, the turbulent motion with the high eddy diffusivity is dominant in momentum and mass transfer and considered to determine value of $\overline{c}$ without the influence of the factors treated as above.

In comparison with the Newtonian fluid flow, the viscoelastic fluid flow shows steep velocity and concentration gradient layers corresponding to low diffusivity. The velocity gradient for the viscoelastic fluid flow is almost same with that of Virk's velocity profile instead of the laminar profile. We can also observe a lower velocity even in the wall vicinity, compared to the laminar profile. In order to elucidate this behavior, we consider the velocity profile in terms of the stress balance equation for the fully-developed channel flow of the viscoelastic fluid. The total stress, τ, balance equation in the turbulent channel flow of the viscoelastic fluid is follows,

$$\tau = \mu \frac{\mathrm{d}\overline{u}}{\mathrm{d}y} - \rho\overline{u'v'} + \overline{\tau^{(\mathrm{ve})}}. \tag{1}$$

Here, $\overline{\tau^{(\mathrm{ve})}}$ means the mean viscoelastic stress. If the turbulent modulation level is high, the Reynolds shear stress is equal almost zero in Eq. 1. In that case, the following equation is derived from the integral of Eq. 1 in normalization with the inner scale from the wall position to y,

$$\overline{u^+} = y^+ - \int_0^{y^+} \overline{\tau^{(\mathrm{ve})+}} \mathrm{d}y^+. \tag{2}$$

In the present experiment, viscoelastic fluid flow shows the almost zero Reynolds shear stress independent on y as shown later. Therefore, we can say from Eq. 2 that the occurrence of the viscoelastic stress triggers the decrease of $\overline{u}$ from the laminar state. In addition, the relation between the wall friction coefficient, C_f, and the mean velocity profile is described as

$$C_f = \frac{2\mathrm{Re}_\tau}{\int_0^{\mathrm{Re}_\tau} \overline{u^+} \mathrm{d}y^+}. \tag{3}$$

From Eq. 3, it is understandable that the mean velocity reduction due to the high viscoelastic stress leads to the moderate *DR*% as shown in Table 1, whereas the Virk's velocity profile was observed in the high *DR*% case around 70%∼80% with the low viscoelastic stress.

INSTANTANEOUS DYE CONCENTRATION FIELD

To investigate how convection in the channel flow forms instantaneous dye concentration field spatially, Figure 4 shows typical contour map of concentration fluctuating component for the flow of Newtonian and viscoelastic fluids. Vector of velocity fluctuation (u', v') in normalization with u_τ and ν are also shown in the same figure. From the Newtonian fluid case in Fig. 4(a), typical turbulent diffusion can be seen and distributes random velocity vector consisting of multiscale eddies. As especially prominent feature, Q_2 ($u' < 0$, $v' > 0$) and Q_4 ($u' > 0$, $v' < 0$) motions stand out in spatial distribution. According to these motions at (A) and (B) regions in the figure, c' and u' occupy the same space, and so these are associated with the same behavior of Reynolds shear stress and wall-normal turbulent mass flux. Therefore, it is concluded that these turbulence motions actively transfer mass to away from the dosing wall, and then result in the thick dye concentration boundary layer reaching at $y^+ = 571$.

For the viscoelastic fluid case in Fig. 4(b), velocity vectors show hierarchically large-scale wavy motions with inclination existing in $\Delta y \cong 20 - 30$, which are completely different from the motion caused by characteristic eddies observed in Newtonian fluid flow. Whereas Q_2 and Q_4 motions are attenuated, Q_1 ($u' > 0$, $v' > 0$) and Q_3 ($u' < 0$, $v' < 0$) motions become prominent, and result in almost zero of the averaged Reynolds shear stress. Mass transport depicts occurrence of c' with same sign for u' at the same place in space, as shown in (C) and (D) regions. The dye concentration fluctuation does not follow small v' at all, but Q_2 and Q_4 motions with regards to spatially large v' transfer c' in the same manner as u' (see e.g., (C) and (D) regions in the figure). However, the wall-normal turbulent mass flux is smaller than that of Newtonian fluid flow, so that the dye concentration layer formed of a thin area of $y^+ \leq 99$. If the turbulence motion transfers mass in the wall-normal direction inside the thin dye concentration layer, intense c' occurs in wide range in space due to the steep concentration gradient.

SPECTRA ANALYSIS

Analysis of the power spectra of fluctuating components and the co-spectra of the Reynolds shear stress and wall-normal turbulent mass flux ($E_{u'u'}$, $E_{v'v'}$, $E_{c'c'}$, $E_{u'v'}$ and $E_{c'v'}$) allows us to quantitatively evaluate contribution from various scales. The pre-multiplied spectra and co-spectra of these values in the x-directional wave number are shown in Figs. 5-8 for the case of Newtonian and viscoelastic fluids and its integral in $\log(k_x^+)$, (averaged values in physical space of the x-direction and in time), is displayed on the right with DNS data. Inner normalization with u_τ and ν is used and the contour interval is a tenth of maximum counter level in the figure. Basically, turbulence statistics not relating to c' for the Newtonian fluid flow shows quite similar profile in comparison with previous DNS results because of the factors explained in the previous section.

From the behavior of the Newtonian fluid flow in Fig. 5, it is confirmed that the peak of $k_x^+ E_{u'u'}^+$ and $k^+ E_{c'c'}^+$ with the white cross on the map shows $k_x^+ \simeq 0.0012$ at $y^+ \simeq 10$ corresponding to the buffer layer with a large velocity gradient. The wave-number range of their energetic modes is broadband and its area is concentrated in the wall vicinity. On the other hand, the broad peak of highly energetic modes of $k_x^+ E_{v'v'}^+$ is locating in around higher wave number for remote region from the wall as well the peak position because of the blocking effect by the wall. A gradual decrease of rms values with the wall distance beyond the peak can be observed. This implies that the turbulence motion in the Newtonian fluid flow has high eddy diffusivity for mass leading to the relaxation of $\overline{c}$ gradient below the outer edge of $\overline{c}$ distribution.

As can be observed from Fig. 6, the viscoelastic fluid flow clearly brings out the high c'^+_{rms} in the layer with the large $\overline{c}$ gradient, which is consistent with the findings of concentration field. In addition, the peak position of fluctuating components shifts to the bulk flow, compared with that of the Newtonian fluid flow. The similar behavior has been also observed at different wall turbulences of the viscoelastic fluid by many previous studies: the experimental investigation of heat transfer at channel or pipe flows (Kawaguchi *et al.* (2002) and Li *et al.* (2004)), the numerical investigation of passive scalar transport in a channel flow (Gupta *et al.* (2005)) and the experimental verification in a polymer drag-reduced turbulent boundary layer (Somandepalli *et al.* (2010)). While lower wave-number modes are dominant in $k_x^+ E_{u'u'}^+$ and $k_x^+ E_{c'c'}^+$ far from the wall, $k_x^+ E_{v'v'}^+$ shows higher wave-number modes. The extent of those energetic modes is also smaller in comparison with the Newtonian fluid flow.Therefore, it is concluded that the turbulence fluctuation in the viscoelastic fluid flow consists of multiscale only around one characteristic length scale and an strong anisotropy between velocity fluctuations appears in the wave-number space.

Figures 7 and 8(a) of the Newtonian fluid case present the pre-multiplied co-spectra distribution centered on low wave number in wider wave-number range from the buffer layer to the log layer. Their integrals in $\log(k_x^+)$ increase from the wall and decrease gradually after the peak towards the channel center. The wave number and wall-normal distance of the peak $k_x^+ E_{u'v'}^+$ are $k_x^+ \simeq 0.0012$ and $y^+ \simeq 37$, respectively. This observation is consistent with the previous study (del Álamo & Jiménez (2003)). The peak wave number of $k_x^+ E_{c'v'}^+$ is identical for $k_x^+ E_{u'v'}^+$, but the peak location at $y^+ = 23$ is more near the wall. The difference of the peak location is because the high Schmit number effect induces the diffusion layer thinner than the viscous layer. The high Schmit number effect also appears in an difference between energetic areas and can explain an observation of dye concentration fluctuation in smaller scale than velocity fluctuations. However, dominant wave-number modes of $k_x^+ E_{u'v'}^+$ and $k_x^+ E_{c'v'}^+$ are identical fundamentally and coincide with the feature of Q_2 and Q_4 motions in large scale discussed in the investigation for instantaneous field.

For wall turbulence of viscoelastic fluid, the peak wave number of $k_x^+ E_{u'v'}^+$ and $k_x^+ E_{c'v'}^+$ is lower than that of the Newtonian fluid and the peak location is far away from the wall. Figure 7(b) exhibits attenuation of $k_x^+ E_{u'v'}^+$ on the map, which results in the zero Reynolds shear stress. It should be noted that the coherence between u' and v' in the drag-reducing flow decreases monotonically in all wave number due to the phase modulation between fluctuating velocity components (Hara *et al.* (2017)). Incidentally, the contour line shows a double-hump in low and high wave-number modes that are originating from the peak value of pre-multiplied spectra of $u'u'$ and $v'v'$, respectively. The phase modulation between c' and v' can be also understand from the feature in Fig. 4(b) and its coherence decreases uniformly. However, $k_x^+ E_{c'v'}^+$ shows high energetic area centered in low wave-number modes at the wall vicinity. This coincides with the behavior of the pre-multiplied spectra for the intense c' appearing in the thin dye concentration boundary layer. Therefore, it is concluded that hierarchically large-scale wavy motions transfer mass and form the thin dye concentration layer that contributes to the magnitude difference between the Reynolds shear stress and wall-normal turbulent mass flux.

CONCLUSION

The present paper investigated the turbulence structure in a turbulent channel flow of viscoelastic fluid by simultaneous PIV and PLIF measurements. Hierarchically wavy motions with inclination in large scale mainly contribute to the mass transfer. Cross spectral analysis revealed that phase is spatially modulated in the streamwise velocity fluctuation and the dye concentration for the wall-normal velocity fluctuation. These features reflect reduction of the Reynolds shear stress and wall-normal turbulent mass flux in a spectral description. The resulting thinner dye concentration layer enhances the magnitude of dye concentration fluctuation. This leads to the magnitude difference between the Reynolds shear stress and wall-normal turbulent mass flux.

ACKNOWLEDGMENTS

A part of this study was nationally supported by the research grants (17J08520) of the JSPS Japan.

REFERENCES

Adrian, R. J., Christensen, K. T. & Liu, Z.-C. 2000 Analysis and interpretation of instantaneous turbulent velocity fields. *Experiments in Fluids* **29** (3), 275–290.

del Álamo, J. C. & Jiménez, J. 2003 Spectra of the very large anisotropic scales in turbulent channels. *Physics of Fluids* **15** (6), L41–L44.

Benson, M. J., Elkins, C. J., Mobley, P. D., Alley, M. T. & Eaton, J. K. 2010 Three-dimensional concentration field measurements in a mixing layer using magnetic resonance imaging. *Experiments in Fluids* **49** (1), 43–55.

Fu, Z., Otsuki, T., Motozawa, M., Kurosawa, T., Yu, B. & Kawaguchi, Y. 2014 Experimental investigation of polymer diffusion in the drag-reduced turbulent channel flow of inhomogeneous solution. *International Journal of Heat and Mass Transfer* **77**, 860–873.

Gillis, A. M., Gray, M. & Burstein, D. 2000 Diffusion coefficients of MRI contrast agents in cartilage. *46th Annual Meeting, Orthopaedic Research Society* .

Gnielinski, V. 1976 New equations for heat and mass transfer in turbulent pipe and channel flow. *International Journal of Chemical Engineering* **16** (2), 359–368.

Gupta, V. K., Sureshkumar, R. & Khomami, B. 2005 Passive scalar transport in polymer drag-reduced turbulent channel flow. *American Institute of Chemical Engineers Journal* **51** (7), 1938–1950.

Hara, S., Ii, R., Tsukahara, T. & Kawaguchi, Y. 2017 Analysis of an organized turbulent structure using a pattern recognition technique in a drag-reducing surfactant solution flow. *International Journal of Heat and Fluid Flow* **63**, 56–66.

Iwamoto, K., Suzuki, Y. & Kasagi, N. 2002 Reynolds number effect on wall turbulence: toward effective feedback control. *International Journal of Heat and Fluid Flow* **23** (5), 678–689.

Kawaguchi, Y., Segawa, T., Feng, Z. & Li, P. 2002 Experimental study on drag-reducing channel flow with surfactant additives–spatial structure of turbulence investigated by PIV system. *International Journal Heat and Fluid Flow* **23** (5), 700–709.

Kays, W. M. 2012 *Convective heat and mass transfer*. Tata McGraw-Hill Education.

Kozuka, M., Seki, Y. & Kawamura, H. 2009 DNS of turbulent heat transfer in a channel flow with a high spatial resolution. *International Journal of Heat and Fluid Flow* **30** (3), 514–524.

Li, F. C., Kawaguchi, Y. & Hishida, K. 2004 Investigation on the characteristics of turbulence transport for momentum and heat in a drag-reducing surfactant solution flow. *Physics of Fluids* **16** (9), 3281–3295.

Matsumoto, T., Hara, S., Tsukahara, T. & Kawaguchi, Y. 2017 Instantaneous turbulent structure relating to momentum and scalar transport in a reducing channel flow with surfactant additives. In *ASME 2017 Fluids Engineering Division Summer Meeting*, pp. V01CT18A004–V01CT18A004. American Society of Mechanical Engineers.

Ptasinski, P. K., Boersma, B. J., Nieuwstadt, F. T. M., Hulsen, M. A., Van den Brule, B. H. A. A. & Hunt, J. C. R. 2003 Turbulent channel flow near maximum drag reduction: simulations, experiments and mechanisms. *Journal of Fluid Mechanics* **490**, 251–291.

Somandepalli, V. S. R., Hou, Y. X. & Mungal, M. G. 2010 Concentration flux measurements in a polymer drag-reduced turbulent boundary layer. *Journal of Fluid Mechanics* **644**, 281–319.

Virk, P. S. 1975 Drag reduction fundamentals. *American Institute of Chemical Engineers Journal* **21** (4), 625–656.

White, C. M. & Mungal, M. G. 2008 Mechanics and prediction of turbulent drag reduction with polymer additives. *Annual Review of Fluid Mechanics* **40**, 235–256.

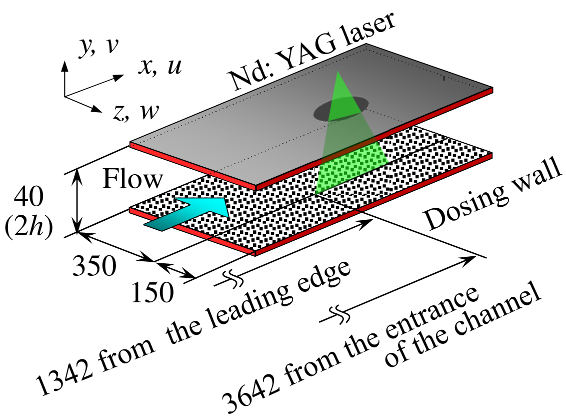

Figure 1. Schematic diagram of simultaneous PIV and PLIF measurement on permeable wall in test section. Identical solution with laser dye is dosed slowly from the wall in constant mass flow rate condition.

Table 1. Experimental parameters, where the friction Reynolds number is defined as $\mathrm{Re}_\tau = u_\tau h/\nu$ and the 99% dye concentration layer thickness is δ_c. The percentage of drag reduction at identical Reynolds number $DR\%$ is defined as $(C_f^{Newtonian} - C_f^{Viscoelastic})\ /\ C_f^{Newtonian} \times 100$, where superscript means type of fluid.

	Re	Re_τ	$DR\%$	δ_c^+
Newtonian fluid	1.0×10^4	309	-	571
Viscoelastic fluid	1.2×10^4	248	40.8	99

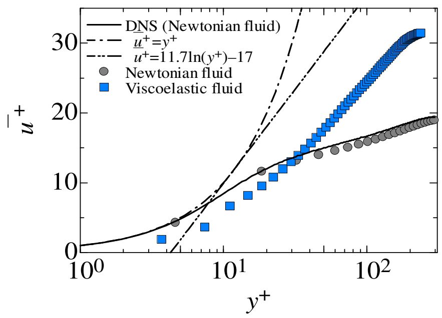

Figure 2. Averaged streamwise velocity profile. DNS data for Newtonian fluid flow at Re = 10039 Iwamoto *et al.* (2002).

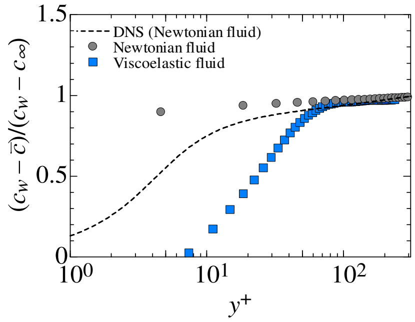

Figure 3. Averaged dye concentration profile. DNS data for Newtonian fluid flow at the uniform heat-flux heating condition at Re = 14124 and Pr =7.0 Kozuka *et al.* (2009).

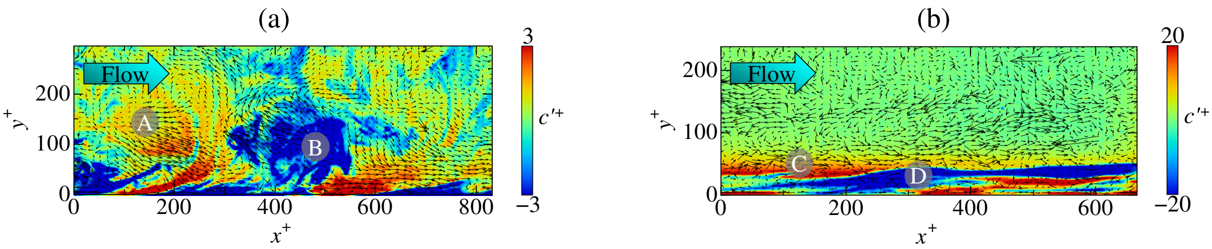

Figure 4. Typical instantaneous dye concentration field with vector of velocity fluctuation in turbulent channel flow. (a) Newtonian fluid, (b) viscoelastic fluid.

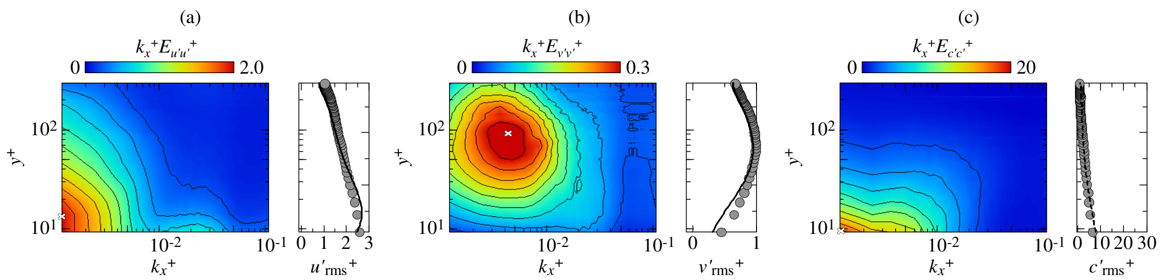

Figure 5. Maps of pre-multiplied power spectra of fluctuating components as a function of wave number and distance from the wall, and those root-mean-square distributions for Newtonian fluid. White cross is placed on the peak value on the map. Solid and dashed lines mean DNS data of Iwamoto *et al.* (2002) and Kozuka *et al.* (2009), respectively. (a) streamwise velocity fluctuation, (b) wall-normal velocity fluctuation, (c) dye concentration fluctuation.

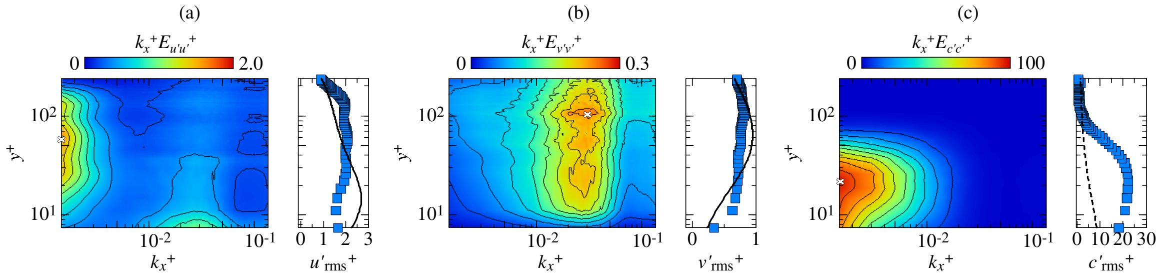

Figure 6. Maps of pre-multiplied power spectra of fluctuating components as a function of wave number and distance from the wall, and those root-mean-square distributions for viscoelastic fluid. White cross is placed on the peak value on the map. Solid and dashed lines mean DNS data of Iwamoto *et al.* (2002) and Kozuka *et al.* (2009), respectively. (a) streamwise velocity fluctuation, (b) wall-normal velocity fluctuation, (c) dye concentration fluctuation.

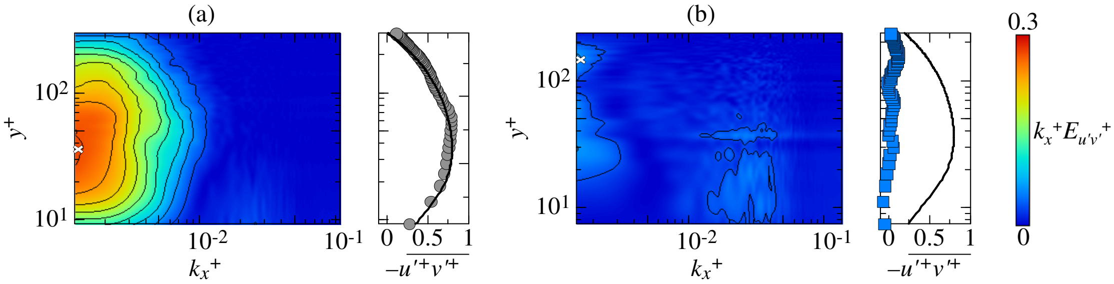

Figure 7. Maps of pre-multiplied co-spectra of Reynolds shear stress as a function of wave number and distance from the wall, and averaged Reynolds shear stress distributions with the solid line of DNS data for Newtonian fluid flow at Re = 10039 (Iwamoto *et al.* (2002)). White cross is placed on the peak value on the map. (a) Newtonian fluid, (b) viscoelastic fluid.

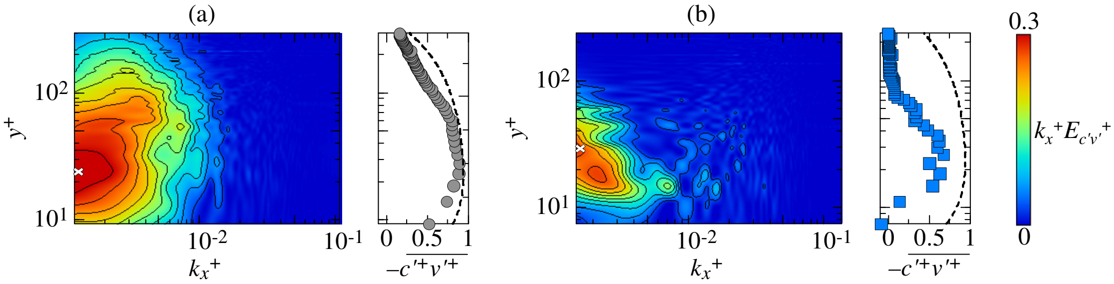

Figure 8. Maps of pre-multiplied co-spectra of wall-normal turbulent mass flux as a function of wave number and distance from the wall, and averaged wall-normal turbulent mass flux distributions with the dashed line of DNS data for Newtonian fluid flow at the uniform heat-flux heating condition at Re = 14124 and Pr =7.0 (Kozuka *et al.* (2009)). White cross is placed on the peak value on the map. (a) Newtonian fluid, (b) viscoelastic fluid.